Advances in deflectometric form measurement

Marcus Petz, Hanno Dierke, and Rainer Tutsch

Technische Universität Braunschweig, Institut für Produktionsmesstechnik,
Schleinitzstraße 20, 38106 Braunschweig

Abstract Phase measuring deflectometry is an accepted technique for measuring the shape of specular surfaces. While defloctometry is known to provide high sensitivity in the nanometer range, the absolute form measuring accuracy is typically inferior by several orders of magnitude. The comparatively low accuracy of typical implementations of phase measuring deflectometry is determined by several influencing factors. On the one hand, many system models used do not consider all relevant system parameters, such as refraction in the display substrate or its flatness deviation. On the other hand, due to the complex system geometry, many calibration procedures are susceptible to deviations due to low condition numbers of the mathematical problems. To increase the absolute accuracy of phase measuring deflectometry, the authors have analyzed in detail the calibration procedures, the measurement process, and the evaluation algorithms and have made numerous extensions and optimizations. The present contribution gives an overview of the obtained findings and the applied measures. The performance of the approach is evaluated based on measurements of challengingly curved measurement objects. Based on these selected objects, form measurement deviations of better than 1 µm are documented.

Keywords Deflectometry, specular surface, phase shifting, structured illumination, system calibration, photogrammetry

DOI: 10.58895/ksp/1000124383-13 erschienen in:

Forum Bildverarbeitung 2020

DOI: 10.5445/KSP/1000124383 | https://www.ksp.kit.edu/site/books/m/10.58895/ksp/1000124383/

1 Introduction

Phase measuring deflectometry is accepted as a highly sensitive method for full-field form measurement of specular surfaces. However, the accuracy of the absolute form measurement has so far significantly lagged behind the sensitivity due to systematic influences. As part of the work presented here, the deflectometric calibration, measurement, and evaluation processes were subjected to a number of extensions and optimizations in order to obtain an absolute form measurement accuracy in the sub-micrometer range for typical optical functional surfaces with diameters of 50 mm to 100 mm.

Deflectometry is based on the observation of reference patterns whose images are reflected by the surface under test and are thereby distorted depending on the surface geometry. In most practical applications of phase measuring deflectometry liquid crystal displays are utilized to represent the required reference patterns. A main concern is therefore to optimize the spatial coding strategies and to characterize the non-ideal display properties, such as characteristic curve, topography, and refractive power.

Another important aspect is the geometric calibration of the whole setup, especially the relative orientation of measuring camera and liquid crystal display. As typically the camera is not able to directly observe the display without the beam deflection of a specular object, the calibration process requires a specular calibration object. Ideally, the properties of that object, especially its spatial location and orientation, are known. However, approaches with a high degree of self-calibration, similar to the established bundle adjustment techniques used in protogrammetry, have also been reported in the literature. The authors have therefore investigated the potential of approaches with a high degree of freedom and have compared their results with information obtained from other strategies.

The surface reconstruction in deflectometry involves the integration of the measured surface gradients. Furthermore, this process requires additional information to regularize the deflectometric problem. In the performed work, the approach of using at least two different relative orientations of object and reference pattern was used, which has been proposed in [1]. But even then, there are several different strategies for processing the obtained measurement data.

In the following, numerous aspects of the deflectometric calibration, measurement, and evaluation processes are discussed as an overview and hints to realizations are given that have proven to be advantageous during the investigations.

2 Measurement setup

The used measurement setup shown in Figure 2.1 implements the approach of using at least two different relative orientations of object and reference pattern to resolve the ambiguities, which are typical for the deflectometric problem [1]. For realizing this internal distance reference, the setup features a directly driven linear stage of type Standa 8MTL1301-170-LEn1-200, which has a travel of 170 mm with an encoder resolution of 50 nm and a bidirectional repeatability of ± 0.5 µm. As realization of the reference patterns a medical-grade grayscale liquid crystal display of type NEC MD211G5 with a resolution of 2048 x 2560 pixels is used.

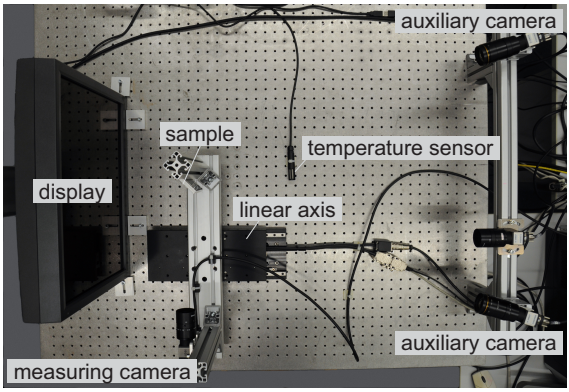

Figure 2.1: Deflectometric measurment setup according to the approach of using two different relative orientations of object and display in order to resolve ambiguities [1].

In contrast to earlier systems used by the authors, for the first time the measuring camera and the test object instead of the display were mounted on the linear stage. As a result, the moving masses are re-

duced and, in addition, the display can be attached very firmly to the optical table with numerous supports, so that the structure has good long-term stability. On the downside, however, it was noticed that different masses of the measurement objects coupled to the linear stage result in very small but detectable tilting movements, which should be addressed in future optimizations.

An essential element of the measurement setup is the stereophotogrammetric auxiliary camera system, which enables an in-situ determination of the display topography as one of the most important deviation influences. The used cameras are all of type IDS UI-3060CP, have a resolution of 2.35 megapixels and are equipped with high-quality lenses. A 35 mm Ricoh FL-BC3518-9M lens is used on the measuring camera, the auxiliary camera system has 16 mm lenses of type Kowa LM16XC.

3 Pattern properties and display calibration

The known phase shifting technique using a heterodyne method for deconvolution of the phase information was subjected to a detailed statistical analysis in order to maximize the robustness on the one hand – i. e. to minimize the probability of deconvolution errors – and on the other hand to increase the statistical deviations of the spatial coding – i. e. minimizing the effects of phase noise. A mathematically well-founded optimality criterion for setting the three wavelengths of the heterodyne method at a given base wavelength was formulated and verified. Compared to conventional approaches, an optimized wavelength ratio can reduce the probability of unwrapping errors by several orders of magnitude [2].

To minimize the statistical deviations of the spatial coding of the display surface by means of phase shifting, it is important to use the most favorable fringe period in each situation. The phase noise model developed by Fischer et al. [3] [4] and the propagation of the deviations into the object space provide an experimental method for determining the optimal wavelength in the respective situation. Figure 3.1 shows that an increase of the wavelength leads to a steady reduction in the phase deviation due to the associated increase in fringe contrast. But considering the physical wavelength

in the display surface, the minimum noise level of the spatial coding is achieved at a comparatively small, clearly definable wavelength. Based on this statistical model, also a strategy to fuse phase measurements with different base wavelengths was implemented, in order to locally achieve the most favorable noise level possible on strongly or unevenly curved object surfaces.

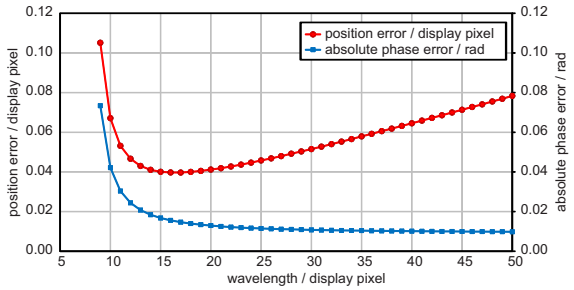

Figure 3.1: Experimentally determined minimization of the statistical position error for a given measurement situation by determining the optimal pattern period.

Since the refraction in the glass substrate of liquid crystal displays represents a significant systematic influence of deviation in deflectometric measurements, special attention was paid to formulating a model describing this influence and an experimental procedure for its determination, which is as precise as possible and at the same time easy to apply. An approach previously followed by the authors has been subjected to extensive revision and refinement. As a result, a partly self-calibrating procedure for determining the refractive properties of the transparent layer was developed, which eliminates or reduces uncertainties of the previous implementation [5] [6]. Following this method, the refractive influence of liquid crystal displays can be characterized and taken into account with previously unattainable accuracy.

Great effort was made to determine the topography of liquid crystal displays. As part of this, various measurement approaches to determine the topography were compared and influences on the topography (gravity, temperature, ...) and temporal variations of the topography were analyzed. As a result, a photogrammetric method

was implemented that enables the determination of the topography directly in the deflectometric setup and, by using the phase coding also used for the deflectometric measurement process, enables a direct determination of the position of each individual display pixel. The auxiliary camera system shown in Figure 2.1 serves primarily for this purpose.

Influences on the optical detection, such as in particular the refraction in the glass substrate, are considered and corrected during the topography measurement. After performing comparative investigations of different approaches, the description of the display topography is currently based on 2D polynomials, which enable the efficient determination of individual surface points of the display and the associated surface normals during the measurement process. The implemented model also enables higher-order deviations to be taken into account, such as the influence of the arc length due to stronger flatness deviations or local deviations in the position of individual pixels. However, it should be noted that these effects, which are typically in the low single-digit micrometer range, cannot be reliably differentiated from noise or higher-frequency residual errors of the camera system due to the large measurement volume (the screen diagonal is more than 540 mm).

4 System calibration

Regarding the system calibration, it was of particular interest to what extent a simultaneous calibration of different components offers advantages or disadvantages compared to a sequential calibration. It was found that simultaneous approaches seem to work well and achieve a high internal accuracy, but that when compared with external reference data, the solutions found this way often show strong deviations, so that the external accuracy or correctness of the calibration is not satisfactory. The behavior observed and supported by simulation calculations indicates that the associated systems of equations converge, but are very susceptible to even small, systematic disturbances due to low condition numbers. A calibration routine is therefore preferred that breaks down the process into individual

sub-steps and, if possible, uses reference information that is not part of the deflectometric arrangement itself.

In a first step a classic photogrammetric calibration with ten parameters for describing the intrinsic orientation of all involved cameras is carried out using calibrated targets. In this step, in order to avoid systematic errors, it is important to ensure that the spectral distribution of the light source that is used to illuminate the targets is as similar as possible to that of the background lighting of the liquid crystal display.

The topography of the liquid crystal screen is then determined directly in the deflectometric setup, but independently of the deflectometric principle by means of a stereophotogrammetric camera system, as shown in Figure 2.1. In this step, external information, in particular about the pixel spacing of the display as obtained from a measurement by means of an optical coordinate measuring machine, is ideally used to increase the accuracy.

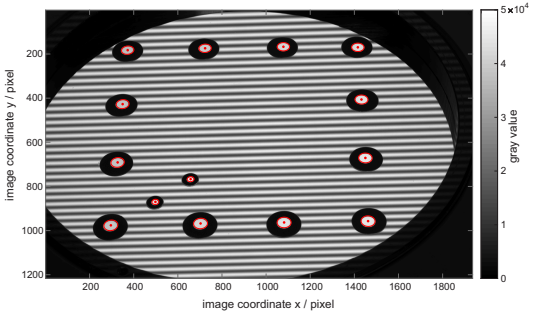

Figure 4.1: Calibration mirror with attached photogrammetric targets. For better visualization, the shown image was composed of two seperate images, one with exposure adjusted to the fringe pattern and one only showing the photogrammetric targets. The red overlay indicates the results from ellipse detection.

To determine the relative orientation of the measuring camera and the (not directly observable) display, a plane mirror as shown in Figure 4.1 with a diameter of 100 mm is used, which is equipped with photogrammetry targets. The relative distances of the targets were measured by an optical coordinate measuring machine and allow the

determination of the mirror position by using only one camera. The mirror can therefore be freely positioned during the calibration process. Ideally, several measurements with different orientations of the mirror are combined, to maximize the robustness and the accuracy. But even in this case it has proven to be disadvantageous to make use of the obvious overdetermination of the problem and to have one or more of the orientation parameters of the calibration mirror be adjust as free parameters.

This sequential procedure has proven to be very flexible and, thanks to the different sources of information, also enables systematic residual errors to be identified, so that these can be further minimized through iterative improvements to components, calibration routines and algorithms.

5 Measurement results

An assessment of the form measurement deviation that can be achieved using the developed approaches and procedures is currently based on the measurement of selected flat and, in particular, spherical test specimens. When selecting the test specimens, it was the declared aim to utilize the usable dynamic range of the created measurement setup as far as possible with regard to the maximum curvature and dimension of the test objects. Using simulation calculation, a convex, spherical test object with an aperture diameter of 50 mm and a radius of curvature of -100 mm was identified as the extreme value, which corresponds to a high aperture ratio of f/1. The other end of the specimen range is formed by a concave specimen with an aperture diameter of also 50 mm and a radius of curvature of 4 inches. Furthermore, one concave and one convex test specimen each with twice the radius of curvature resulting in an aperture ratio of f/2 and a plane mirror, all with an aperture diameter of 50 mm, were used for the qualification measurements.

The measurement data show that this selection of objects can cover unfavorable borderline cases of the measurement setup. Figure 5.1 shows the resulting cases of maximum and minimum used display area. Thus, global effects of the display (shape deviation, viewing angle dependency, ...) as well as local effects (pixel structure, stripe

pattern, ...) impact the measurements as potential sources of deviation.

The absolute radii of curvature were determined by a MarSurf LD 120 combined contour and roughness measurement station. The specified form deviations of the test specimens verified by the contour measurements are $\lambda/4$ in the case of the spherical mirrors and $\lambda/10$ for the plane mirror. It therefore seems justified to ascribe most of the deviations described below to the deflectometric measurement.

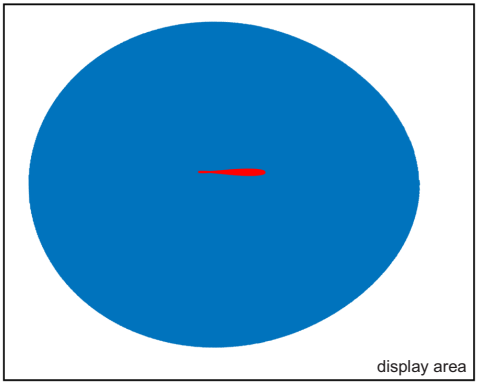

Figure 5.1: Minimal and maximal display observation areas within the range of chosen measurement objects.

Table 1 summarizes the parameters that were achieved on the five test objects in the course of a measurement campaign. It should be emphasized that all measurements were carried out with the system geometry unchanged, i. e. that apart from the sample position no adaptions to the individual properties of the mirrors have been made. For the special case of the plane mirror, only the range of deviations from a best fit plane and the standard deviation of these deviations are listed as parameters. For spherical mirrors, based on guidelines from the field of geometric metrology, a distinction is made between a *probing error size* – in this case the deviation of the radius of the best fit sphere from the reference radius – and a *prob-*

ing error form – here the range of radial deviations from the best fit sphere. In addition, the standard deviation of the radial deviations of this evaluation is given. In order to be able to better assess the influence of the *probing error size* on the *probing error form*, the *probing error total* is also specified, which is the peak-to-valley values of the radial deviations from the spherical surface with the respective reference radius.

Table 1: Measurement deviations achieved on test specimens with different radii of curvature. All mirrors have an aperture diameter of 50 mm. A margin of 1 mm is not taken into account for the evaluation. Further explanation of the parameters in the text.

nominal radius	reference radius (mm)	best fit radius (mm)	probing err. size (µm)	probing err. form (µm)	standard deviation (µm)	probing err. total (µm)
∞ (flat)	∞	–	–	(0.24)	0.06	0.24
8 inch (concave)	203.114	203.138	24.09	0.32	0.05	0.40
4 inch (concave)	101.513	101.502	-11.14	0.61	0.10	0.71
-200 mm (convex)	-200.073	-200.02	52.52	0.47	0.08	0.65
-100 mm (convex)	-99.941	-99.926	14.54	0.92	0.13	1.16

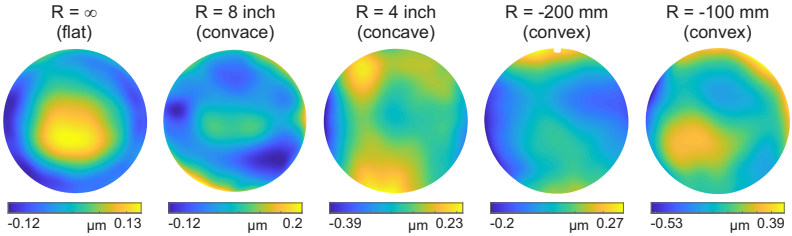

Figure 5.2: Visual representation of the local deviation from the best fit element as taken for probing error form according to Table 1. The color coding of the individual images is selected differently, and each encompasses the range of the corresponding probing error form.

The results in Table 1 show that the *probing error form* for all test objects is less than 1 µm. As stated, these values are the range of all radial deviations. For the standard deviation, here comparable to

the RMS error, values in the two-digit to lower three-digit nanometer range are achieved. The *probing error size* is consistently in the double-digit micrometer range, which however cannot not be interpreted in a quantitative way, since only more or less small sections of a complete spherical surface were measured. The indication of the probing error with respect to a spherical surface of the respective reference radius appears more meaningful, whereby an additional spherical deviation is added to the *probing error form*. As a result, the *probing error total* is on average approx. 25% higher than the *probing error form*.

In Figure 5.2, the radial deviations from the best fit sphere are shown for each of the five measurements listed. The range of these radial deviations corresponds to the *probing error form* from Table 1. The range of the color coding is chosen differently for the five samples and its interval corresponds to the *probing error form*. Due to the spatial frequencies, the local distribution of the residual deviations appears to be systematic in each case, but differ significantly across the test objects.

To minimize the influence of the integration process on the form measurement, existing integration techniques were further developed and compared. An implemented simulation environment has proven to be extremely valuable, as it allowed to use synthetic data to understand higher-order deviations and to minimize their impact. In addition to a local integration approach – which correctly takes into account the imaging distortions of the measuring camera and, compared to earlier work [1], also eliminates curvature-dependent residual errors through an iterative evaluation – two global, model-based approaches were implemented. With these, a polynomial surface – optionally a conventional 2D polynomial or a Zernike polynomial – is adapted to the measured surface normals, whereby any points from internal distance reference can be used for regularization with variable weighting.

In Figure 5.3, for one of the measurements from Figure 5.2 the results obtained from different integration methods are compared. In principle, only the local approach is able to map higher spatial frequencies, but with regard to the form, all three approaches show very good agreement. With the same polynomial order, however, the Zernike polynomials have a somewhat greater tendency to overshoot

at the edge of the test object, which means that the arithmetic range is usually somewhat larger. The results from Table 1 and Figure 5.2 were calculated using 2D polynomials of order 12.

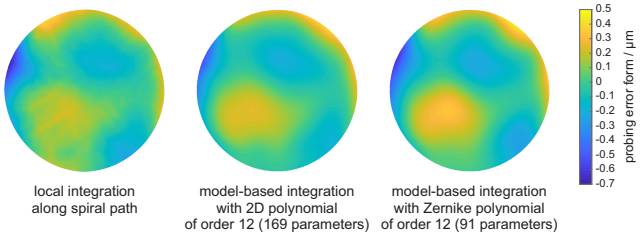

Figure 5.3: Comparison of different integration strategies exemplified by the convex mirror with R_{nom} = -100 mm. The color coding of the individual images is chosen identically and covers the interval [-0.7 µm, 0.5 µm].

6 Summary

A significant improvement of the absolute accuracy of phase measuring deflectometry was achieved by the performed work, which covers a wide range of aspects that contribute to the absolute accuracy. It can be stated that the sub-systems and sub-problems of a deflectometric setup can now be mastered at about the same level as the underlying photogrammetric principle. As a matter of fact, at least some of the remaining deviations can be attributed to not completely corrected optical distortions of the used cameras. These and other systematic residual errors are subject of ongoing investigations.

Acknowledgement

The authors gratefully acknowledge the funding of this work by Deutsche Forschungsgemeinschaft (DFG) under grant Pe1402/6-1.

References

1. M. Petz, "Rasterreflexions-Photogrammetrie – Ein neues Verfahren zur geometrischen Messung spiegelnder Oberflächen," Dissertation, Technische Universität Braunschweig, 2006, Schriftenreihe des Instituts für Produktionsmesstechnik, Band 1, Aachen: Shaker.
2. M. Petz, H. Dierke, and R. Tutsch, "Wellenlängenoptimierung bei Heterodyn-Phasenschiebeverfahren," *tm - Technisches Messen (published online ahead of print)*, 22 Sep. 2020.
3. M. Fischer, M. Petz, and R. Tutsch, "Vorhersage des Phasenrauschens in optischen Messsystemen mit strukturierter Beleuchtung," *tm - Technisches Messen*, vol. 79, no. 10, pp. 451–458, 2012.
4. M. Fischer, M. Petz, and T. R., "Modellbasierte Rauschvorhersage für Streifenprojektionssysteme – Ein Werkzeug zur statistischen Analyse von Auswertealgorithmen," *tm - Technisches Messen*, vol. 84, no. 2, pp. 111–122, 2017.
5. M. Petz, H. Dierke, and R. Tutsch, "Photogrammetric determination of the refractive properties of liquid crystal displays," *tm - Technisches Messen*, vol. 86, no. 6, pp. 319–324, 2019.
6. H. Dierke, M. Petz, and R. Tutsch, "Photogrammetrische Bestimmung der Brechungseigenschaften von Flüssigkristallbildschirmen," in *Forum Bildverarbeitung 2018*, Längle, T. and Puente León, F. and Heizmann, M., Ed. Karlsruhe: KIT Scientific Publishing, 2018, pp. 13–24.